IEEE Access
Multidisciplinary | Rapid Review | Open Access Journal

Received June 10, 2020, accepted June 21, 2020, date of publication June 23, 2020, date of current version July 20, 2020.

Digital Object Identifier 10.1109/ACCESS.2020.3004485

Fast Angle Estimation and Sensor Self-Calibration in Bistatic MIMO Radar With Gain-Phase Errors and Spatially Colored Noise

GUANQUN SHENG[1], HAN WANG[2], (Member, IEEE), FANG-QING WEN[3], AND XINHAI WANG[4]

[1]College of Computer and Information on Technology, China Three Gorges University, Yichang 443002, China
[2]Institute of Data Science, City University of Macau, Macau 999078, China
[3]National Demonstration Center for Experimental Electrical and Electronic Education, Yangtze University, Jingzhou 434023, China
[4]Nanjing Marine Radar Institute, Nanjing 211153, China

Corresponding author: Fang-Qing Wen (wenfangqing@yangtzeu.edu.cn)

This work was supported in part by the National Natural Science Foundation of China under Grant 61701046 and Grant 61871258.

ABSTRACT Multiple-input multiple-output (MIMO) radars are essential in many Internet-of-Things (IoT) applications. Gain-phase error calibration is an important branch in MIMO radar. Existing calibration algorithms are only suitable for white Gaussian noise scenario, however, spatially colored noise is more practical in engineering implementation. In this paper, we stress the problem of direction finding and sensor self-calibration in a bistatic MIMO radar in the co-exist of unknown gain-phase error and spatially colored noise, and a covariance tensor-based parallel factor analysis (PARAFAC) estimator is proposed. To suppress the spatially colored noise and exploit the multi-dimensional structure of the array measurement, a covariance tensor is firstly established and the temporal cross-correlation operation is followed. Then the PARAFAC decomposition is carried out to obtain the factor matrices. Thereafter, automatically paired direction estimation is achieved via least squares. Finally, the element-wise multiply/divide technique and the Lagrange multipliers are adopted to obtain the gain-phase error vectors. The algorithm is analyzed in terms of identifiability and Cramer-Rao bound (CRB). Numerical simulations results show the effectiveness and improvement of the proposed estimator.

INDEX TERMS Gain-phase error, spatially colored noise, colocated multiple-input multiple output radar, parallel factor analysis, sensor calibration.

I. INTRODUCTION

Internet-of-Things (IoT) is one of the most important infrastructures in our future smart cities. The concept of IoV can be spread in a wide area, e.g., Internet-of-Vehicles [1], [2], Internet-of-Industry [3], [4]. It is really a complex system that integrates sensors, wireless communications, computations, big data, *et al.* The super integration ability enables IoT to provide safe, comfortable and convenient life for human begin. Sensors are the most fundamental units in IoT, they are usually utilized to sense the necessary information, and thus assist to make suitable command to the IoT system. Source positioning using sensor or sensor array is an interesting topic in IoV with numerical applications [1], [2]. For example, to provide unmanned drive service, to offer real-time navigation and to call for emergency rescue. This topic is especially attractive in colocated multiple-input multiple output (MIMO) radars, since it always involves high-dimensional signal processing and multiple parameter estimation. According to its sensor distribution, colocated MIMO radar can be divided into two different classes, namely monostatic configurations and multi-static geometries. Direction finding is the most fundamental task in colocated MIMO radars. In a monostatic configuration, it means to get the direction-of-arrival (DOA) of the targets, whereas in a multi-static configuration, it requires to get both the DOA and direction-of-departure (DOD) of the targets.

Till now, various estimation strategies have been proposed for MIMO radars, such as multiple signal classification (MUSIC) [5], Capon, subspace fitting, estimating signal

The associate editor coordinating the review of this manuscript and approving it for publication was Zhenyu Zhou.

parameters via rotational invariance technique (ESPRIT) [6], least squares (LS) [7], maximum likelihood (ML) [8], tensor approaches [9]–[12], optimization-aware algorithms [13]–[15]. With respect to tensor approaches, there are two main tensor decomposition frameworks, called higher-order singular value decomposition (HOSVD) and parallel factor analysis (PARAFAC) decomposition. The former is highly similar to the traditional eigendecomposition method but can obtain subspaces that are more accurate than the traditional ones, the latter factorizes a tensor to rank one tensors, i.e., factor matrices than form the tensor. Usually, tensor-based approaches provides better estimation performance than matrix-based ones, as they can explore the inherent multi-dimensional nature of the tensor measurement. However, as illustrated in the literature, these algorithms can only work well in the presence of ideal scenarios, e.g., white Gaussian noise, well-calibrated sensors. Nevertheless, non-ideal backgrounds often encounter MIMO radar, such as spatially colored noise, gain-phase errors, sensor mutual coupling [16]. Usually, mutual coupling effect can be easily eliminated via using sparse sensor manifold (such as coprime arrays [17], [18]), but the effect of gain-phase errors and spatially colored noise cannot be easily removed. Many efforts have been devoted to solve these two problems.

When unknown gain-phase errors exist in MIMO radar, the transmit/receive direction matrices would be coupled with the gain-phase matrices, thus results in decreased estimated performance. To this end, some self-calibration algorithms have been presented. In [19], a reduced-dimensional MUSIC method has been given. It is suitable for arbitrary sensor manifold, but it needs exhaustive spectrum grid search, which means it is computationally inefficient and cannot avoid the drawback of off-grid problem [8]. In [20], an ESPRIT-like algorithm has been proposed, which is capable to provide closed-form solution for joint DOD and DOA estimation. A propagator method has been driven in [21], which does not require the eigen-decomposition calculation in [19], [20]. Another low-complexity calibration algorithm has been proposed in [22], which relies on two well-calibrated sensors. However, the subspace-based method are complex, since they often involve high-dimensional optimization problem. Taking the tensor nature of the measurement into consideration, a PARAFAC estimator has been proposed in [23]. It first perform PARAFAC on the array signal to estimate the factor matrices, and then it estimate the gain-phase errors via the Lagrange multiplier method. Based on the previous estimated gain-phase error, joint DOD and DOA estimation are obtained via least square algorithm. The PARAFAC estimator offers more accurate performance than the matrix-based approaches in [19]–[22]. However, the gain-phase error estimations cannot avoid the cumulative effective. All the above mentioned methods require at least two well-calibrated sensors at both the transmit and receive (T/R) end. An improved PARAFAC version has been proposed in [24], which only require one calibrated sensor in the T/R end. However, the array manifold must be strict non-linear, making it is unsuitable for engineering application.

When faced with unknown spatially colored noise, the covariance matrix of which is no longer scaled with the identity matrix, thus the traditional methods will invalid. To obtain the noiseless covariance matrix, several de-noising frameworks have been proposed. In [25]–[28], the spatial cross-correlation strategies have been utilized. Herein, the transmit array is grouped into two or more non-overlapped subarrays, as the array noise (after matched filtering) corresponding to different transmit antenna is uncorrelated, the noise's spatial covariance matrix is full of zeros. In [29]–[30], the temporal cross-correlation schemes have been derived, in which the array measurements are divided into two parts, each part associate with different pulse index. As the noise is temporal uncorrelated, the cross-correlation of the two parts is equal to a zero matrix. In [31], the covariance differencing methods have been discussed, the spatially colored noise is suppressed via covariance differencing, however, the signal counterpart keeps invariant under the differencing transformation. Generally, the spatial cross-correlation strategies are computationally economic, however, they always provide poor estimation performance, as they cannot avoid the virtual aperture loss. Both the temporal cross-correlation algorithms and the covariance differencing approaches can make full use of the virtual degree-of-freedom of a MIMO radar, but the covariance differencing approaches are more complex than the former, since the estimated angles are the unambiguous, so they require additional pair calculation.

It should be emphasized that, as mentioned previously, the gain-phase error problem and the spatially colored noise problem have been stressed separately in MIMO radar, but they are more likely to appear together in engineering application. To the best of our knowledge, no work has taking this problem into consideration. Inspired by the tensor structure of the array measurement from a MIMO radar, a fast PARAFAC estimator is given for sensor calibration and direction finding. The main contributions of this paper are summarized as follow:

- We take both gain-phase error and spatially colored noise into consideration. As far as we know, this is the first time that both imperfect scenarios are discussed. To solve this problem, the spatially colored noise is firstly eliminated, then tensor decomposition is performed for signal analysis. After which parameter estimation and gain-phase error calibration are carried out.
- We proposed a novel PARAFAC algorithm for joint DOD and DOA estimation. The noiseless covariance measurement is rearranged into a third-order PARAFAC model, a fast PARAFAC decomposition is proposed to obtain the corrupt direction matrices. Joint DOD and DOA estimation is accomplished via solving a LS fitting problem, thus to obtain closed-form and automatically paired solutions.

- We proposed a new gain-phase error calibration algorithm. The element-wise multiply/divide technique is estimate the gain errors, while the Lagrange multipliers is utilized to obtain the phase error. Unlike the pervious calibration algorithm, the proposed method is free from the cumulative effect. Besides, the algorithm is analyzed in terms of identifiability and Cramer-Rao bound (CRB).
- We validate the effectiveness of the proposed algorithm via numerical simulation. Compared with existing calibration algorithms, the proposed algorithm is robust against spatially colored noise, thus it provides more accurate parameter estimations. Numerical computer examples validate the effectiveness of the proposed estimator.

Notations: Lowercase bold letters, e.g., $\boldsymbol{a}$, capital bold letters, e.g., $\boldsymbol{A}$, and boldface calligraphic letters, e.g., $\boldsymbol{\mathcal{A}}$, denote vectors, matrices and tensors, respectively. $(\cdot)^T$, $(\cdot)^H$, $(\cdot)^{-1}$, and $(\cdot)^\dagger$ account for transpose, Hermitian transpose, inverse, and pseudo-inverse, respectively; $\|\cdot\|_F$ denotes the Frobenius norm. $\otimes$ and $\odot$ account for the Kronecker product and the KhatriRao product, respectively; phase $(\cdot)$ returns the phase of a vector in radian; vec $(\cdot)$ denotes vectorization; $E[\cdot]$ is to get the mathematical expectation of a variable. diag $(\boldsymbol{a})$ returns a diagonal matrix with the diagonal entities are the elements of $\boldsymbol{a}$. $\delta(\cdot)$ is the delta function with $\delta(0) = 1$ and $\delta(n \neq 0) = 0$. The element-wise divide and element-wise multiply are denoted by ./ and .$\times$, respectively.

II. PRELIMINARIES AND SIGNAL MODEL

A. TENSOR PRELIMINARIES

Before we give the signal model, we introduce some preliminaries concerning tensors and tensor operations (please refer to [12] and the references therein for more details).

Definition 1 (Matrix Unfolding): The mode-n matrix unfolding operation of an N-order tensor $\boldsymbol{\mathcal{X}} \in \mathbb{C}^{I_1 \times \cdots I_N}$ is denoted by $[\boldsymbol{\mathcal{X}}]_n$, where the $(i_1, \ldots, i_n)$-th element of $\boldsymbol{\mathcal{X}}$ maps to the (i_n, j)-th element of $[\boldsymbol{\mathcal{X}}]_n$, with $j = 1 + \sum_{k=1,k\neq n}^{N} (i_k - 1) J_k$ and $J_k = \prod_{m=1,m\neq n}^{k-1} I_m$.

Definition 2 (Mode-n Tensor-Matrix Product): The mode-n product of $\boldsymbol{\mathcal{X}} \in \mathbf{C}^{I_1 \times I_2 \times \cdots I_N}$ by a matrix $\boldsymbol{A} \in \mathbf{C}^{J_n \times I_n}$, is denoted by $\boldsymbol{\mathcal{Y}} = \boldsymbol{\mathcal{X}} \times_n \boldsymbol{A}$, in mode-n matrix unfolding format, it can be expressed as $[\boldsymbol{\mathcal{Y}}]_n = \boldsymbol{A}[\boldsymbol{\mathcal{X}}]_n$.

Definition 3 (The Properties of the Mode Product): The properties of the mode product are shown as follows:

$$\begin{aligned} \boldsymbol{\mathcal{X}} \times_n \boldsymbol{A} \times_m \boldsymbol{B} &= \boldsymbol{\mathcal{X}} \times_m \boldsymbol{B} \times_n \boldsymbol{A}, \quad m \neq n \\ \boldsymbol{\mathcal{X}} \times_n \boldsymbol{A} \times_m \boldsymbol{B} &= \boldsymbol{\mathcal{X}} \times_n (\boldsymbol{B}\boldsymbol{A}), \quad m = n \end{aligned} \tag{1}$$

$$\left[\boldsymbol{\mathcal{X}} \times_1 (\boldsymbol{A}_1) \times_2 \cdots (\boldsymbol{A}_N)\right]_n = \boldsymbol{A}_n [\boldsymbol{\mathcal{X}}]_n [\boldsymbol{A}_N \otimes \cdots \boldsymbol{A}_{n+1} \otimes \boldsymbol{A}_{n-1} \cdots \otimes \boldsymbol{A}_1]^T \tag{2}$$

Definition 4 (PARAFAC Decomposition): The PARAFAC decomposition of an N-order tensor $\boldsymbol{\mathcal{X}}$ with rank-K is given by

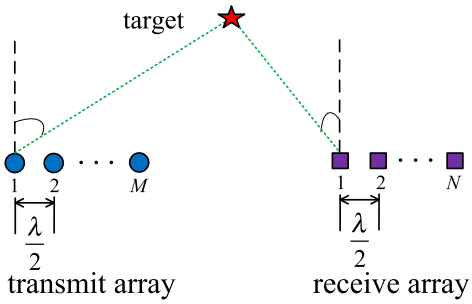

FIGURE 1. Illustration of a bistatic MIMO radar.

$$\boldsymbol{\mathcal{X}} = \boldsymbol{\mathcal{I}} \times_1 (\boldsymbol{A}_1) \times_2 (\boldsymbol{A}_2) \times_3 \cdots \times_N (\boldsymbol{A}_N) \tag{3}$$

where $\boldsymbol{\mathcal{I}} \in \mathbb{C}^{K \times K \cdots K}$ is a diagonal tensor with the $(k, k, \ldots, k)$-th entities are ones and zeros elsewhere, $\boldsymbol{A}_n \in \mathbb{C}^{I_n \times K}$ is a full column rank matrix. In matrix format, (3) can be expressed as

$$[\boldsymbol{\mathcal{X}}]_n = \boldsymbol{A}_n [\boldsymbol{A}_N \odot \cdots \boldsymbol{A}_{n+1} \odot \boldsymbol{A}_{n-1} \cdots \odot \boldsymbol{A}_1]^T \tag{4}$$

Definition 5 (Generalized Tensorization of a PARAFAC model): For a PARAFAC decomposition model in (3), let the order sets $\mathbb{Q}_j = \{o_{j,1}, o_{j,2}, \ldots, o_{j,M}\}$ for $j = 1, 2, \ldots, J$ be a partitioning of the dimensions $\mathbb{Q} = \{1, 2, \ldots, N\}$, the generalized tensorization of $\boldsymbol{\mathcal{X}}$ is denoted by a new tensor $\boldsymbol{\mathcal{X}}_{\mathbb{Q}_1, \mathbb{Q}_2, \ldots, \mathbb{Q}_J} \in \mathbb{C}^{T_1 \times T_2 \times \cdots T_J}$ with

$$\boldsymbol{\mathcal{X}}_{\mathbb{Q}_1, \mathbb{Q}_2, \ldots, \mathbb{Q}_J} = \boldsymbol{\mathcal{I}} \times_1 (\boldsymbol{B}_1) \times_2 (\boldsymbol{B}_2) \times_3 \cdots \times_J (\boldsymbol{B}_J) \tag{5}$$

where $\boldsymbol{B}_j = \boldsymbol{A}_{o_{j,1}} \odot \boldsymbol{A}_{o_{j,2}} \odot \boldsymbol{A}_{o_{j,M_j}}$, T_j is the row dimension of $\boldsymbol{B}_j$.

B. SIGNAL MODEL

We consider a general bistatic MIMO radar scenario, in which the MIMO radar is equipped with M transmit sensors and N receive sensors, as illustrated in Fig. 1. To simplify the data model, we assume both the transmit array and the receive array are uniform linear arrays (ULA) with half-wavelength distributing. Besides, we suppose that the transmit sensors omit mutually orthogonal pulse waveforms $s_m(t)$, $m = 1, 2, \ldots, M$, i.e.,

$$\int_0^T s_m(t)\, s_n^*(t) dt = \delta(m - n) \tag{6}$$

where t is the fast time index, T is the pulse duration. Assume that K targets appearing in the far-field of MIMO radar, the DOD and DOA for the k-th target are denoted by φ_k and θ_k, respectively. The reflected echo from the k-th target is

$$r_k(t, \tau) = b_k(\tau)\, \boldsymbol{a}_t^T(\varphi_k)\, \boldsymbol{s}(t) \tag{7}$$

where τ is the pulse index, $b_k(\tau) = b_k e^{j2\pi f_k \tau}$ is the target characteristic coefficient corresponding to the k-th target, b_k and f_k stand for the reflection amplitude and Doppler frequency shift of the k-th target $\boldsymbol{a}_t(\varphi_k) = \left[1, e^{-j\pi \sin(\varphi_k)}, \ldots, e^{-j(M-1)\pi \sin(\varphi_k)}\right]^T \in \mathbb{C}^{M \times 1}$ is the associate transmit steering vector, $s(t) =$

$[s_1(t), s_2(t), \ldots, s_M(t)]^T$ is the waveform vector. The captured signal at the receive end can be expressed as

$$\boldsymbol{x}(t,\tau) = \sum_{k=1}^{K} b_k(\tau)\,\boldsymbol{a}_r(\theta_k)\,\boldsymbol{a}_t^T(\varphi_k)\,\boldsymbol{s}(t) + \boldsymbol{w}(t,\tau) \quad (8)$$

where $\boldsymbol{a}_r(\theta_k) = \left[1, e^{-j\pi\sin(\theta_k)}, \ldots, e^{-j(N-1)\pi\sin(\theta_k)}\right]^T \in \mathbb{C}^{N\times 1}$ is the associate receive steering vector, $\boldsymbol{w}(t,\tau)$ is the array noise, which is assumed to be spatially correlated with unknown covariance matrix $\boldsymbol{Q}$, i.e.,

$$E\left\{\boldsymbol{w}(t_1,\tau)\,\boldsymbol{w}^H(t_2,\tau)\right\} = \boldsymbol{Q}\delta(t_1 - t_2) \quad (9)$$

Matching $\boldsymbol{x}(t,\tau)$ with $s_m(t)$ yields [30]

$$\begin{aligned}\boldsymbol{y}_m(\tau) &= \int_0^T \boldsymbol{x}(t,\tau)\,s_m^*(t)dt \\ &= \sum_{k=1}^{K} b_k(\tau)\,\boldsymbol{a}_r(\theta_k)\,\boldsymbol{a}_t^m(\varphi_k) + \boldsymbol{n}_m(\tau)\end{aligned} \quad (10)$$

where $\boldsymbol{a}_t^m(\varphi_k)$ is the m-th entity in $\boldsymbol{a}_t(\varphi_k)$, $\boldsymbol{n}_m(\tau) = \int_0^T \boldsymbol{w}(t,\tau)\,s_m^*(t)dt$ is the matched array noise. Let $\boldsymbol{y}(\tau) = \left[\boldsymbol{y}_1^T(\tau), \boldsymbol{y}_2^T(\tau), \ldots, \boldsymbol{y}_M^T(\tau)\right]^T$ and $\boldsymbol{n}(\tau) = \left[\boldsymbol{n}_1^T(\tau), \boldsymbol{n}_2^T(\tau), \ldots, \boldsymbol{n}_M^T(\tau)\right]^T$, then we have

$$\begin{aligned}\boldsymbol{y}(\tau) &= \sum_{k=1}^{K} b_k(\tau)\left[\boldsymbol{a}_t(\varphi_k) \otimes \boldsymbol{a}_r(\theta_k)\right] + \boldsymbol{n}(\tau) \\ &= \left[\boldsymbol{A}_t \odot \boldsymbol{A}_r\right]\boldsymbol{b}(\tau) + \boldsymbol{n}(\tau)\end{aligned} \quad (11)$$

where $\boldsymbol{b}(\tau) = [b_1(\tau), b_2(\tau), \ldots, b_K(\tau)]^T$ is the target reflection coefficient matrix, $\boldsymbol{A}_t = [\boldsymbol{a}_t(\varphi_1), \boldsymbol{a}_t(\varphi_2) \ldots, \boldsymbol{a}_t(\varphi_K)] \in \mathbb{C}^{M\times K}$ and $\boldsymbol{A}_r = [\boldsymbol{a}_r(\theta_1), \boldsymbol{a}_r(\theta_2), \ldots, \boldsymbol{a}_r(\theta_K)] \in \mathbb{C}^{N\times K}$ are the corresponding transmit direction matrix and receive direction matrix, respectively. (11) ignores the sensor errors in MIMO radar. Taking the gain-phase error in both the transmit array and receive array, (11) is re-written as follows [19]

$$\begin{aligned}\boldsymbol{y}(\tau) &= \left[(\boldsymbol{C}_t\boldsymbol{A}_t) \odot (\boldsymbol{C}_r\boldsymbol{A}_r)\right]\boldsymbol{b}(\tau) + \boldsymbol{n}(\tau) \\ &= \left[\tilde{\boldsymbol{A}}_t \odot \tilde{\boldsymbol{A}}_r\right]\boldsymbol{b}(\tau) + \boldsymbol{n}(\tau) \\ &= \tilde{\boldsymbol{A}}\boldsymbol{b}(\tau) + \boldsymbol{n}(\tau)\end{aligned} \quad (12)$$

where $\boldsymbol{C}_t = diag\{\boldsymbol{c}_t\}$, $\boldsymbol{C}_r = diag\{\boldsymbol{c}_r\}$, $\tilde{\boldsymbol{A}}_t = \boldsymbol{C}_t\boldsymbol{A}_t$ and $\tilde{\boldsymbol{A}}_r = \boldsymbol{C}_r A_r$, $\tilde{\boldsymbol{A}} = \tilde{\boldsymbol{A}}_t \odot \tilde{\boldsymbol{A}}_r$. Assume the first m_t transmit sensors and the first n_r receive sensors have been well-calibrated, then the gain-phase error coefficient vectors corresponding to the transmit sensors and the receive sensors are denoted by $\boldsymbol{c}_t = \left[1, 1, \ldots, 1, \rho_t^{m_t+1}, \ldots, \rho_t^M\right]$ and $\boldsymbol{c}_r = \left[1, 1, \ldots, 1, \rho_r^{n_r+1}, \ldots, \rho_r^N\right]$, with m_t and n_r ones in them, respectively, where $\rho_{t/r}^n = g_{t/r}^n e^{jp_{t/r}^n}$, $g_{t/r}^n \in \mathbb{R}$ and $p_{t/r}^n \in \mathbb{R}$ are the associate gain error and phase error, respectively. Namely,

$$\begin{cases}\boldsymbol{C}_t = \boldsymbol{G}_t\boldsymbol{P}_t \\ \boldsymbol{C}_r = \boldsymbol{G}_r\boldsymbol{P}_r\end{cases} \quad (13)$$

where $\boldsymbol{G}_t = diag\left\{1, 1, \ldots, 1, g_t^{m_t+1}, \ldots, g_t^M\right\}$, $\boldsymbol{P}_t = diag\{1, , 1, \ldots, 1p_t^{m_t+1}, \ldots, p_t^M\}$, $\boldsymbol{G}_r = diag\{1, 1, \ldots, 1, g_r^{n_r+1}, \ldots, g_r^N\}$, $\boldsymbol{P}_r = diag\left\{1, 1, \ldots, 1, p_r^{n_r+1}, \ldots, p_r^N\right\}$. Suppose that the target Doppler frequencies are different, then the covariance matrix of $\boldsymbol{y}(\tau)$ is given by

$$\boldsymbol{R}_y = E\left\{\boldsymbol{y}(\tau)\,\boldsymbol{y}^H(\tau)\right\} = \tilde{\boldsymbol{A}}\boldsymbol{R}_b\tilde{\boldsymbol{A}}^H + \boldsymbol{R}_n \quad (14)$$

where $\boldsymbol{R}_b = E\left\{\boldsymbol{b}(\tau)\,\boldsymbol{b}^H(\tau)\right\}$ is the covariance matrix of the target reflection coefficient, which is a diagonal matrix, $\boldsymbol{R}_n = E\left\{\boldsymbol{n}(\tau)\,\boldsymbol{n}^H(\tau)\right\}$ is the noise covariance matrix. Now we focus on the noise counterpart, note that $\boldsymbol{n}(\tau)$ can also be expressed as

$$\boldsymbol{n}(\tau) = \int_0^T \boldsymbol{s}^*(t)\,\boldsymbol{w}(t,\tau)\,dt \quad (15)$$

then the noise covariance matrix is given by

$$\begin{aligned}&E\left\{\boldsymbol{n}(\tau)\,\boldsymbol{n}^H(\tau)\right\} \\ &= E\left\{\int_0^T\int_0^T \left[\boldsymbol{s}^*(t_1)\otimes\boldsymbol{w}(t_1,\tau)\right]\left[\boldsymbol{s}^*(t_2)\otimes\boldsymbol{w}(t_2,\tau)\right]^H dt_1dt_2\right\} \\ &= E\left\{\int_0^T\int_0^T \left[\boldsymbol{s}(t_1)\,\boldsymbol{s}(t_2)\right]^T\otimes\left[\boldsymbol{w}(t_1,\tau)\,\boldsymbol{w}^H(t_2,\tau)\right]dt_1dt_2\right\} \\ &= \int_0^T\int_0^T \left[\boldsymbol{s}(t_1)\,\boldsymbol{s}(t_2)\right]^T\otimes E\left\{\left[\boldsymbol{w}(t_1,\tau)\,\boldsymbol{w}^H(t_2,\tau)\right]\right\}dt_1dt_2 \\ &= \int_0^T\int_0^T \boldsymbol{I}\delta(t_1-t_2)\otimes\boldsymbol{Q}\delta(t_1-t_2)\,dt_1dt_2 \\ &= \boldsymbol{I}\otimes\boldsymbol{Q}\end{aligned} \quad (16)$$

where $\boldsymbol{I}$ is an identity matrix. In practice, L snapshots can be collected, i.e., $\tau = \tau_1, \tau_2, \ldots, \tau_L$, and the covariance matrix of $\boldsymbol{y}(\tau)$ can be estimated via

$$\boldsymbol{R}_y = \frac{1}{L}\sum_{l=1}^{L}\boldsymbol{y}(\tau_l)\,\boldsymbol{y}^H(\tau_l) \quad (17)$$

From (16) we observe that the noise covariance is not scaled with the identity matrix, thus traditional subspace methods will fail to work, neither the matrix/tensor decomposition approaches could correctly work. Now we face two problems, how to suppress the spatially colored noise, and how to calibrate the transmit/receive sensors.

III. THE PROPOSED FRAMEWORK

The proposed algorithm can be divided into two main steps: to eliminate the noise first, and to calibrate the sensors follows. In what follows, we will show the details of the two steps.

A. DE-NOISING

As we have reviewed previously, several de-noising strategies are available to eliminate the effect of spatially colored noise. In order not to hurt the virtual aperture of MIMO radar, and taking the computational complexity into consideration,

herein we chose the temporal cross-correlation method. It can be seen that

$$\begin{aligned} & E\left\{\boldsymbol{n}\left(\tau_1\right)\boldsymbol{n}^H\left(\tau_2\right)\right\} \\ &= E\left\{\int_0^T\int_0^T\left[\boldsymbol{s}^*(t_1)\otimes\boldsymbol{w}\left(t_1,\tau_1\right)\right]\left[\boldsymbol{s}^*\left(t_2\right)\otimes\boldsymbol{w}\left(t_2,\tau_2\right)\right]^H dt_1dt_2\right\} \\ &= \int_0^T\int_0^T\left[\boldsymbol{s}\left(t_1\right)\boldsymbol{s}\left(t_2\right)\right]^T\otimes E\left\{\left[\boldsymbol{w}\left(t_1,\tau_1\right)\boldsymbol{w}^H\left(t_2,\tau_2\right)\right]\right\}dt_1dt_2 \\ &= \int_0^T\int_0^T\boldsymbol{I}\delta\left(t_1-t_2\right)\otimes\boldsymbol{Q}\delta\left(t_1-t_2\right)dt_1dt_2 \\ &= \left[\boldsymbol{I}\otimes\boldsymbol{Q}\right]\delta\left(\tau_1-\tau_2\right) \end{aligned} \tag{18}$$

which implies that the noise associate with various pulses are uncorrelated. Inspired by the above result, we divide the matched array measurement into two different subsets, one is $\boldsymbol{Y}_1=[\boldsymbol{y}\left(\tau_1\right),\boldsymbol{y}\left(\tau_2\right),\ldots,\boldsymbol{y}\left(\tau_{L-1}\right)]$, and the other one is $Y_2=[\boldsymbol{y}\left(\tau_2\right),\boldsymbol{y}\left(\tau_3\right),\ldots,\boldsymbol{y}\left(\tau_L\right)]$. According to (18), the covariance matrix of $\boldsymbol{Y}_1$ and $\boldsymbol{Y}_2$ is

$$\tilde{\boldsymbol{R}}_{\boldsymbol{y}}=E\left\{\boldsymbol{Y}_1\boldsymbol{Y}_2^H\right\}=\tilde{\boldsymbol{A}}\tilde{\boldsymbol{R}}_{\boldsymbol{b}}\tilde{\boldsymbol{A}}_n^H \tag{19}$$

where the covariance matrix $\tilde{\boldsymbol{R}}_{\boldsymbol{b}}=E\left\{\boldsymbol{b}\left(\tau_1\right)\boldsymbol{b}^H\left(\tau_2\right)\right\}=diag\left\{b_1e^{j2\pi f_1\Delta\tau},b_2e^{j2\pi f_2\Delta\tau},\ldots,b_Ke^{j2\pi f_K\Delta\tau}\right\},\Delta\tau=\tau_p-\tau_{p+1},p=1,2\ldots,L-1$. It is obvious that the noise term is removed from(19). However, the tensor structure is ignored in (19), to make full use of the multi-dimensional structure, the PARAFAC decomposition is established, which will be shown below.

B. PARAFAC DECOMPOSITION

According to [30], $\tilde{\boldsymbol{R}}_y$ can also be arranged into PARAFAC decomposition model as

$$\tilde{\boldsymbol{\mathcal{R}}}_y=\mathcal{I}_{\times1}\tilde{\boldsymbol{A}}_{t\times2}\tilde{\boldsymbol{A}}_{r\times3}\tilde{\boldsymbol{A}}_{t\times4}^*\left(\tilde{\boldsymbol{A}}_r^*\tilde{\boldsymbol{R}}_{\boldsymbol{b}}\right) \tag{20}$$

In the above PARAFAC decomposition model, $\tilde{\boldsymbol{R}}_b$ is connect with $\tilde{\boldsymbol{A}}_r^*$. Actually, $\tilde{\boldsymbol{R}}_b$ can be combined with any of the factor matrices $\tilde{\boldsymbol{A}}_t,\tilde{\boldsymbol{A}}_r,\tilde{\boldsymbol{A}}_t^*$ and $\tilde{\boldsymbol{A}}_r^*$. In fact, $\tilde{\boldsymbol{R}}_y$ can be interpreted as the symmetrical Hermitian unfolding of $\tilde{\boldsymbol{\mathcal{R}}}_y$. There are two main technique for tensor decomposition, one is Tucker decomposition, and the other one is PARAFAC decomposition. Generally speaking, the PARAFAC decomposition method is superior to Tucker decomposition, since the former can get the estimations of the factor matrices, whereas the latter can only get the improved subspace estimation. In this paper, the PARAFAC decomposition technique is chosen for tensor decomposition. PARAFAC decomposition for the model in (20) tries to solve

$$\left\|\boldsymbol{\mathcal{Z}}-\tilde{\boldsymbol{\mathcal{R}}}_y\right\|_F,\ \boldsymbol{\mathcal{Z}}=\mathcal{I}_{\times1}\hat{\boldsymbol{A}}_{t\times2}\hat{\boldsymbol{A}}_{r\times3}\hat{\boldsymbol{A}}_{t\times4}^*\left(\hat{\boldsymbol{A}}_r^*\hat{\boldsymbol{R}}_b\right) \tag{21}$$

which can be accomplished via quadrilinear alternative least squares (QALA). However, QALS suffers from the slow converge speed. It is well-known that a third-order PARAFAC decomposition model can be solved via the fast algorithm COMFAC [12], [30]. To accelerate the convergence, we construct another PARAFAC decomposition model. Define $\mathbb{Q}_1=\{1\},\mathbb{Q}_2=\{2\},\mathbb{Q}_3=\{3,4\}$, according to **Definition 5**, $\tilde{\boldsymbol{\mathcal{R}}}_y$ can be arranged into a third-order tensor $\boldsymbol{\mathcal{Y}}$ as follows

$$\boldsymbol{\mathcal{Y}}=\mathcal{I}_{\times1}\tilde{\boldsymbol{A}}_{t\times2}\tilde{\boldsymbol{A}}_{r\times3}\tilde{\boldsymbol{A}}_{t,r} \tag{22}$$

where $\tilde{\boldsymbol{A}}_{t,r}=\tilde{\boldsymbol{A}}_t^*\odot\left(\tilde{\boldsymbol{A}}_r^*\tilde{\boldsymbol{R}}_{\boldsymbol{b}}\right)$. Obviously, (22) presents a third-order PARAFAC decomposition model. In mode-n matrix unfolding format (as shown in **Definition 4**), $\boldsymbol{\mathcal{Y}}$ can be rewritten as

$$[\boldsymbol{\mathcal{Y}}]_1^T=\left[\tilde{\boldsymbol{A}}_{t,r}\odot\tilde{\boldsymbol{A}}_r\right]\tilde{\boldsymbol{A}}_t^T \tag{23}$$

$$[\boldsymbol{\mathcal{Y}}]_2^T=\left[\tilde{\boldsymbol{A}}_{t,r}\odot\tilde{\boldsymbol{A}}_t\right]\tilde{\boldsymbol{A}}_r^T \tag{24}$$

$$[\boldsymbol{\mathcal{Y}}]_3^T=\left[\tilde{\boldsymbol{A}}_r\odot\tilde{\boldsymbol{A}}_t\right]\tilde{\boldsymbol{A}}_{t,r}^T \tag{25}$$

For a third-order PARAFAC decomposition model, the trilinear alternating least squares (TALS) technique is an effective solver to estimate the three factor matrices. For the factor matrices $\tilde{\boldsymbol{A}}_t,\tilde{\boldsymbol{A}}_r$ and $\tilde{\boldsymbol{A}}_{t,r}$ in (22), TALS tries to fit the following problems simultaneously

$$\min\left\|[\boldsymbol{\mathcal{Y}}]_1^T-\left[\tilde{\boldsymbol{A}}_{t,r}\odot\tilde{\boldsymbol{A}}_r\right]\tilde{\boldsymbol{A}}_t^T\right\|_F \tag{26}$$

$$\min\left\|[\boldsymbol{\mathcal{Y}}]_2^T-\left[\tilde{\boldsymbol{A}}_{t,r}\odot\tilde{\boldsymbol{A}}_t\right]\tilde{\boldsymbol{A}}_r^T\right\|_F \tag{27}$$

$$\min\left\|[\boldsymbol{\mathcal{Y}}]_3^T-\left[\tilde{\boldsymbol{A}}_r\odot\tilde{\boldsymbol{A}}_t\right]\tilde{\boldsymbol{A}}_{t,r}^T\right\|_F \tag{28}$$

TALS treats two of the factor matrices as known parameters, then it tries to update the rest factor matrix via least squares (LS) technique. TALS update all the factor matrices successively, based on the previously obtained factor matrices. The iterations in TALS will repeat before algorithm convergence. It is assumed that K is known. Otherwise, it can be estimated from some of the existing methods. For the factor matrix $\tilde{\boldsymbol{A}}_t$, the LS solutions is

$$\hat{\boldsymbol{A}}_t^T=\left[\tilde{\boldsymbol{A}}_{t,r}\odot\tilde{\boldsymbol{A}}_r\right]^\dagger[\boldsymbol{\mathcal{Y}}]_1^T \tag{29}$$

where $\tilde{\boldsymbol{A}}_r$ and $\tilde{\boldsymbol{A}}_{t,r}$ are previously estimated in the last iteration. Similarly, the LS updates for $\tilde{\boldsymbol{A}}_r$ and $\tilde{\boldsymbol{A}}_{t,r}$ are given by

$$\hat{\boldsymbol{A}}_r^T=\left[\tilde{\boldsymbol{A}}_{t,r}\odot\tilde{\boldsymbol{A}}_t\right]^\dagger[\boldsymbol{\mathcal{Y}}]_2^T \tag{30}$$

$$\hat{\boldsymbol{A}}_{t,r}^T=\left[\tilde{\boldsymbol{A}}_r\odot\tilde{\boldsymbol{A}}_t\right]^\dagger[\boldsymbol{\mathcal{Y}}]_3^T \tag{31}$$

To speed up the convergence, we chose the fast version of TALS, the COMFAC algorithm [12], [30], for PARAFAC decomposition. In COMFAC, it first compresses the tensor into a smaller one, and the iterations are process in the low-dimensional space, which quickly converge after only a few iteration.

As it is known to us, matrix decompositions are usually not unique, unless additional constrains are enforced, e.g, orthogonality. Unlike matrix decomposition, PARAFAC decomposition is always unique under mild condition. **Theorem 1** gives the uniqueness condition of PARAFAC decomposition.

For the PARAFAC decomposition model in (22), if the k-rank of the factor matrices $\tilde{\boldsymbol{A}}_t, \tilde{\boldsymbol{A}}_r$ and $\tilde{\boldsymbol{A}}_{t,r}$ (denoted by $kr\left(\tilde{\boldsymbol{A}}_t\right)$, $kr\left(\tilde{\boldsymbol{A}}_r\right)$, and $kr\left(\tilde{\boldsymbol{A}}_{t,r}\right)$, respectively) satisfy

$$kr\left(\tilde{\boldsymbol{A}}_t\right)+kr\left(\tilde{\boldsymbol{A}}_r\right)+kr\left(\tilde{\boldsymbol{A}}_{t,r}\right) \geq 2K+2 \tag{32}$$

then the estimation of $\tilde{\boldsymbol{A}}_t, \tilde{\boldsymbol{A}}_r$ and $\tilde{\boldsymbol{A}}_{t,r}$, denoted by $\hat{\boldsymbol{A}}_t, \hat{\boldsymbol{A}}_r$ and $\hat{\boldsymbol{A}}_{t,r}$, are unique up to permutation and scaling of columns.

The permutation and scaling effect in PARAFAC decomposition can be expressed as

$$\begin{cases} \hat{\boldsymbol{A}}_t = \tilde{\boldsymbol{A}}_t \boldsymbol{\Pi} \boldsymbol{\Delta}_1 + \boldsymbol{E}_1 \\ \hat{\boldsymbol{A}}_r = \tilde{\boldsymbol{A}}_r \boldsymbol{\Pi} \boldsymbol{\Delta}_2 + \boldsymbol{E}_2 \\ \hat{\boldsymbol{A}}_{t,r} = \tilde{\boldsymbol{A}}_{t,r} \boldsymbol{\Pi} \boldsymbol{\Delta}_3 + \boldsymbol{E}_3 \end{cases} \tag{33}$$

where $\boldsymbol{\Pi}$ is a permutation matrix (as shown in (33), all the estimated factor matrices share the same permutation matrix), $\boldsymbol{E}_1$, $\boldsymbol{E}_2$, and $\boldsymbol{E}_3$ stand for the fitting errors, $\boldsymbol{\Delta}_1$, $\boldsymbol{\Delta}_2$, and $\boldsymbol{\Delta}_3$ are scaling matrices, which are diagonal matrices with $\boldsymbol{\Delta}_1 \boldsymbol{\Delta}_2 \boldsymbol{\Delta}_3 = \boldsymbol{I}_k$.

C. ANGLE ESTIMATION

Once $\hat{\boldsymbol{A}}_t$ and $\hat{\boldsymbol{A}}_r$ have been achieved, the LS technique can be utilized again to obtain direction estimation. It is obvious that the phase of $\boldsymbol{a}_t(\varphi_k)$ is

$$-\text{phase}\left(\boldsymbol{a}_t(\varphi_k)\right) = \left[0, \pi \sin\left(\boldsymbol{\varphi}_k\right), \ldots, \pi (M-1) \sin\left(\boldsymbol{\varphi}_k\right)\right]^T \tag{34}$$

which has linear characteristic. Let $\tilde{\boldsymbol{a}}_t(\varphi_k)$ be the k-th column of $\tilde{\boldsymbol{A}}_t$, and let $\bar{\boldsymbol{a}}_t(\varphi_k)$ be the vector comprimes the first m_t element of $\tilde{\boldsymbol{a}}_t(\varphi_k)$. Since there are at least two well-calibrated sensors in both the transmit/receive array, and let $\boldsymbol{h}_t = -\text{phase}\left(\bar{\boldsymbol{a}}_t(\varphi_k)\right)$, it is easy to find

$$\boldsymbol{P}_t \boldsymbol{b} = \boldsymbol{h}_t \tag{35}$$

with

$$\boldsymbol{P}_t = \begin{bmatrix} 1 & 0 \\ 1 & \pi \\ \vdots & \vdots \\ 1 & (m_t-1)\pi \end{bmatrix}, \quad \boldsymbol{b} = \begin{bmatrix} b_0 \\ b_1 \end{bmatrix} \tag{36}$$

where $\boldsymbol{b}_0$ is a scaler that we do not care about. Let the estimation of $\boldsymbol{h}_t$ is $\hat{\boldsymbol{h}}_t$. The LS solution of $\boldsymbol{b}$ is

$$\hat{\boldsymbol{b}} = \boldsymbol{P}_t^{\dagger} \hat{\boldsymbol{h}}_t \tag{37}$$

Let $\hat{b}_1$ be the estimated b_1, the k-th DOD can be estimated via

$$\varphi_k = \arcsin\left(\hat{b}_1\right) \tag{38}$$

In a similar way, we can get the receive gain-phase error matrix and the k-th DOA. As we pointed out previously, $\hat{\boldsymbol{A}}_t$ and $\hat{\boldsymbol{A}}_r$ share the same permutation matrix, the estimated DOD and DOA are paired automatically.

D. SENSOR CALIBRATION

In what follows, we only explain the principle of sensor calibration and angle estimation from the estimated transmit direction matrix $\hat{\boldsymbol{A}}_t$. Firstly, we focus on gain error vectors estimation. For the first column and the second column of $\hat{\boldsymbol{A}}_t$, denoted as $\hat{\boldsymbol{a}}_t(\varphi_1)$, $\hat{\boldsymbol{a}}_t(\varphi_2)$. According to(33), we have

$$\begin{cases} \hat{\boldsymbol{a}}_t(\varphi_1) \approx \boldsymbol{G}_t \boldsymbol{P} \boldsymbol{a}_t(\varphi_a) \\ \hat{\boldsymbol{a}}_t(\varphi_2) \approx \boldsymbol{G}_t \boldsymbol{P} \boldsymbol{a}_t(\varphi_b) \end{cases}, \quad a, b \in \{1, 2, \ldots, K\} \tag{39}$$

Then, we construct

$$\begin{cases} \hat{\boldsymbol{a}}_t(\varphi_1) ./ \hat{\boldsymbol{a}}_t(\varphi_2) = \boldsymbol{a}_t(\Delta) \\ \hat{\boldsymbol{a}}_t(\varphi_1) .\times \hat{\boldsymbol{a}}_t^*(\varphi_2) = \boldsymbol{G}_t^2 \boldsymbol{a}_t(\Delta) \end{cases} \tag{40}$$

where $\Delta = \varphi_a - \varphi_b$. Thereafter, the transmit gain error vector can be estimated via

$$\hat{\boldsymbol{g}}_t = \sqrt{\left(\hat{\boldsymbol{a}}_t(\varphi_1) .\times \hat{\boldsymbol{a}}_t^*(\varphi_2)\right) ./ \left(\hat{\boldsymbol{a}}_t(\varphi_1) ./ \hat{\boldsymbol{a}}_t(\varphi_2)\right)} \tag{41}$$

Next we will focus on phase error estimation. Let $\boldsymbol{C}_{t,1}$ and $\boldsymbol{C}_{t,2}$ are the diagonal matrices consisted of the first and last $M-1$ entities of c_t. Define $\boldsymbol{U}_t = diag\{\boldsymbol{u}_t\} = \boldsymbol{C}_{t,1} \boldsymbol{C}_{t,2}^{-1}$. Let $\tilde{\boldsymbol{A}}_{t,1}$ and $\tilde{\boldsymbol{A}}_{t,2}$ denotes the first and last $M-1$ rows of $\tilde{\boldsymbol{A}}_t$. It is obvious that the following invariant properties are established

$$\boldsymbol{U}_t \tilde{\boldsymbol{A}}_{t,1} = \tilde{\boldsymbol{A}}_{t,2} \boldsymbol{\Phi}_t \tag{42}$$

where $\boldsymbol{\Phi}_t = diag\left(e^{j\pi \sin\varphi_1}, e^{j\pi \sin\varphi_2}, \ldots, e^{j\pi \sin\varphi_K}\right)$. There are two unknown matrices in (42), to estimate them we need to solve

$$\min_{\boldsymbol{U}_t, \boldsymbol{\Phi}_t} \left\| \boldsymbol{U}_t \tilde{\boldsymbol{A}}_{t,1} - \tilde{\boldsymbol{A}}_{t,2} \boldsymbol{\Phi}_t \right\|_F \tag{43}$$

Following the Lagrange multiplier in [23], we can get

$$\hat{\boldsymbol{u}}_t = \boldsymbol{V}_t^{-1} \boldsymbol{E}_t \left(\boldsymbol{E}_t^T \boldsymbol{V}_t^{-1} \boldsymbol{E}_t\right)^{-1} \boldsymbol{h}_t \tag{44}$$

where $\boldsymbol{V}_t = \left(\boldsymbol{I} - \tilde{\boldsymbol{A}}_{t,1} \tilde{\boldsymbol{A}}_{t,1}^{\dagger}\right) \odot \left(\tilde{\boldsymbol{A}}_{t,2}^* \tilde{\boldsymbol{A}}_{t,2}^T\right)$, $\boldsymbol{E}_t$ consists of the first m_t-1 columns of a $(M-1)\times(M-1)$ identity matrix, $\boldsymbol{h}_t$ is a m_t-1 column vector with all the entities are ones. According to the structure of $\boldsymbol{u}_t$, the gain-phase error of the p-th ($p = m_t+1, m_t+2, \ldots, M$) element c_t^p is given by

$$c_t^p = 1 \Big/ \prod_{q=m_t}^{p} \boldsymbol{u}_t(q) \tag{45}$$

where $\boldsymbol{u}_t(q)$ denotes the q-th element of $\boldsymbol{u}_t$, from which we can get the phase error of the transmit gain-error phase error vector. It can be seen from (45) that the estimated gain-phase error vector cannot avoid the cumulative effective, this is why we estimate the gain error coefficient from the element-wise operation.

IV. ALGORITHM ANALYSIS

A. IDENTIFIABILITY

The maximum target number that the proposed algorithm can identify is constrained by (32). Usually, we have $kr\left(\tilde{\boldsymbol{A}}_t\right) = M$, $\left(\tilde{\boldsymbol{A}}_r\right) = N, kr\left(\tilde{\boldsymbol{A}}_{t,r}\right) = MN$. Therefore, the proposed algorithm can identify at most $K = (MN+M+N-2)/2$. While the PARAFAC method in [23] can detect $K = (M+N+L-2)/2$ targets, and the ESPRIT approach in [20] can detect $\min\{M(N-2), N(M-2)\}$ targets. Therefore, the proposed method may have lower identifiability than PARAFAC or ESPRIT, but we will show that it has better estimation accuracy than them in the simulation section.

B. STOCHASTIC CRB

We assume the entities of the spatially colored noise covariance matrix $\boldsymbol{Q}$ are parameterized by a vector $\boldsymbol{\sigma} = [\sigma_1, \sigma_2, \ldots, \sigma_{\boldsymbol{P}}]^{\mathrm{T}}$, where $\sigma_p (p = 1,2,\ldots, \boldsymbol{P})$ are real constants. Inspired by [19] and [30], we can get the stochastic CRBs on joint DOD and DOA estimation in the presence of spatially colored noise and gain-phase noise, which are given by

$$\mathrm{CRB}_{\mathrm{STO}}(\theta, \varphi) = \frac{1}{L}\left[\boldsymbol{H} - \boldsymbol{M}\boldsymbol{T}^{-1}\boldsymbol{M}^T\right]^{-1} \tag{46}$$

with

$$\boldsymbol{H} = 2Re\left\{\left(\tilde{\boldsymbol{D}}^H \boldsymbol{\Pi}_{\tilde{\boldsymbol{A}}}^{\perp} \tilde{\boldsymbol{D}}\right) \oplus \left(\breve{\boldsymbol{R}}_{\boldsymbol{b}}^T \otimes 1_{2\times 2}\right)\right\} \tag{47}$$

$$\boldsymbol{M} = 2\mathrm{Re}\left\{\begin{bmatrix} \boldsymbol{J}^T\left(\left(\tilde{\boldsymbol{D}}_{\theta}^H \boldsymbol{\Pi}_{\tilde{\boldsymbol{A}}}^{\perp}\right) \otimes \left(\tilde{\boldsymbol{R}}^{-1}\breve{\boldsymbol{A}}\boldsymbol{R}_{\boldsymbol{b}}\right)^T\right)\tilde{\boldsymbol{Q}}^* \\ \boldsymbol{J}^T\left(\left(\tilde{\boldsymbol{D}}_{\varphi}^H \Pi_{\tilde{\boldsymbol{A}}}^{\perp}\right) \otimes \left(\tilde{\boldsymbol{R}}^{-1}\breve{\boldsymbol{A}}\boldsymbol{R}_{\boldsymbol{b}}\right)^T\right)\tilde{\boldsymbol{Q}}^* \end{bmatrix}\right\} \tag{48}$$

$$\boldsymbol{J} = \left[\mathrm{vec}\{\boldsymbol{e}_1\boldsymbol{e}_1^T\}, \mathrm{vec}\{\boldsymbol{e}_2\boldsymbol{e}_2^T\}, \ldots, \mathrm{vec}\{\boldsymbol{e}_k\boldsymbol{e}_k^T\}\right] \tag{49}$$

$$\boldsymbol{Q} = \left[\mathrm{vec}\{\tilde{\boldsymbol{Q}}_1'\}, \mathrm{vec}\{\tilde{\boldsymbol{Q}}_2'\}, \ldots, \mathrm{vec}\{\tilde{\boldsymbol{Q}}_p'\}\right] \tag{50}$$

where $\tilde{\boldsymbol{D}} = [\tilde{\boldsymbol{D}}_{\theta}, \tilde{\boldsymbol{D}}_{\varphi}]$, $\tilde{\boldsymbol{D}}_{\theta} = \boldsymbol{Q}^{-1/2}\boldsymbol{D}_{\theta}$, $\tilde{\boldsymbol{D}}_{\varphi} = \boldsymbol{Q}^{-1/2}\boldsymbol{D}_{\theta}$. $\boldsymbol{D}_{\theta} = \boldsymbol{C}\left[\boldsymbol{a}_t(\boldsymbol{\varphi}_1) \otimes \frac{\partial \boldsymbol{a}_r(\boldsymbol{\theta}_1)}{\partial \theta_1}, \ldots, \boldsymbol{a}_t(\boldsymbol{\varphi}_K) \otimes \frac{\partial \boldsymbol{a}_r(\boldsymbol{\theta}_K)}{\partial \theta_K}\right]$ and $D_{\boldsymbol{\varphi}} = \boldsymbol{C}\left[\frac{\partial \boldsymbol{a}_t(\boldsymbol{\varphi}_1)}{\partial \varphi_1} \otimes \boldsymbol{a}_r(\boldsymbol{\theta}_1), \ldots, \frac{\partial \boldsymbol{a}_t(\boldsymbol{\varphi}_K)}{\partial \varphi_K} \otimes \boldsymbol{a}_r(\boldsymbol{\theta}_2)\right]$, $\boldsymbol{C} = \boldsymbol{C}_t \otimes \boldsymbol{C}_r$. $\boldsymbol{\Pi}_{\tilde{\boldsymbol{A}}}^{\perp} = \mathbf{I} - \boldsymbol{\Pi}_{\tilde{A}}$ with $\boldsymbol{\Pi}_{\tilde{\boldsymbol{A}}} = \breve{\boldsymbol{A}}\breve{\boldsymbol{A}}^{\dagger}\breve{\boldsymbol{A}} = \boldsymbol{Q}^{-1/2}\tilde{\boldsymbol{A}}$, $\breve{\boldsymbol{R}}_{\boldsymbol{b}} = \boldsymbol{R}_{\boldsymbol{b}}\breve{\boldsymbol{A}}^H\tilde{\boldsymbol{R}}^{-1}\breve{\boldsymbol{A}}\boldsymbol{R}_{\boldsymbol{b}}, \tilde{\boldsymbol{R}} = \boldsymbol{Q}^{-1/2}\tilde{\boldsymbol{R}}_y\boldsymbol{Q}^{-1/2}$, $1_{2\times 2}$ denotes the 2×2 matrix filled with ones. $\tilde{\boldsymbol{Q}}_p' = \boldsymbol{Q}^{-1/2}\boldsymbol{Q}_p'\boldsymbol{Q}^{-1/2}$ and $\boldsymbol{Q}_p' = \frac{\partial \boldsymbol{Q}}{\partial \sigma_p}$.

V. SIMULATION RESULTS AND DISCUSSIONS

To show the effectiveness of the proposed estimator, numerical simulations results are presented. In the simulations, we consider a bistatic MIMO radar configured with M = 8 transmit sensors and N = 8 receive sensors, both of which are ULAs with half-wavelength spacing. The transmit gain-phase error vector is $c_t = [1, 1, 1, 1.21e^{j0.12}, 1.1e^{j0.35}, 0.89e^{j0.98}, 1.35e^{j2.65}, 0.92e^{j1.97}]$ and the receive gain-phase error vector is $c_r = [1, 1, 0.94e^{j1.12}, 1.23e^{j2.35}, 1.49e^{j0.58}, 0.75e^{j0.65}, 0.52e^{j1.22}, 2.1e^{j0.89}]$. Assume that there are K = 3 uncorrelated point target appearing the same range bin of the radar system, and the DOD-DOA pairs are $(20°, 10°)$, $(35°, -15°)$ and $(60°, 0°)$, and L snapshots are collected.

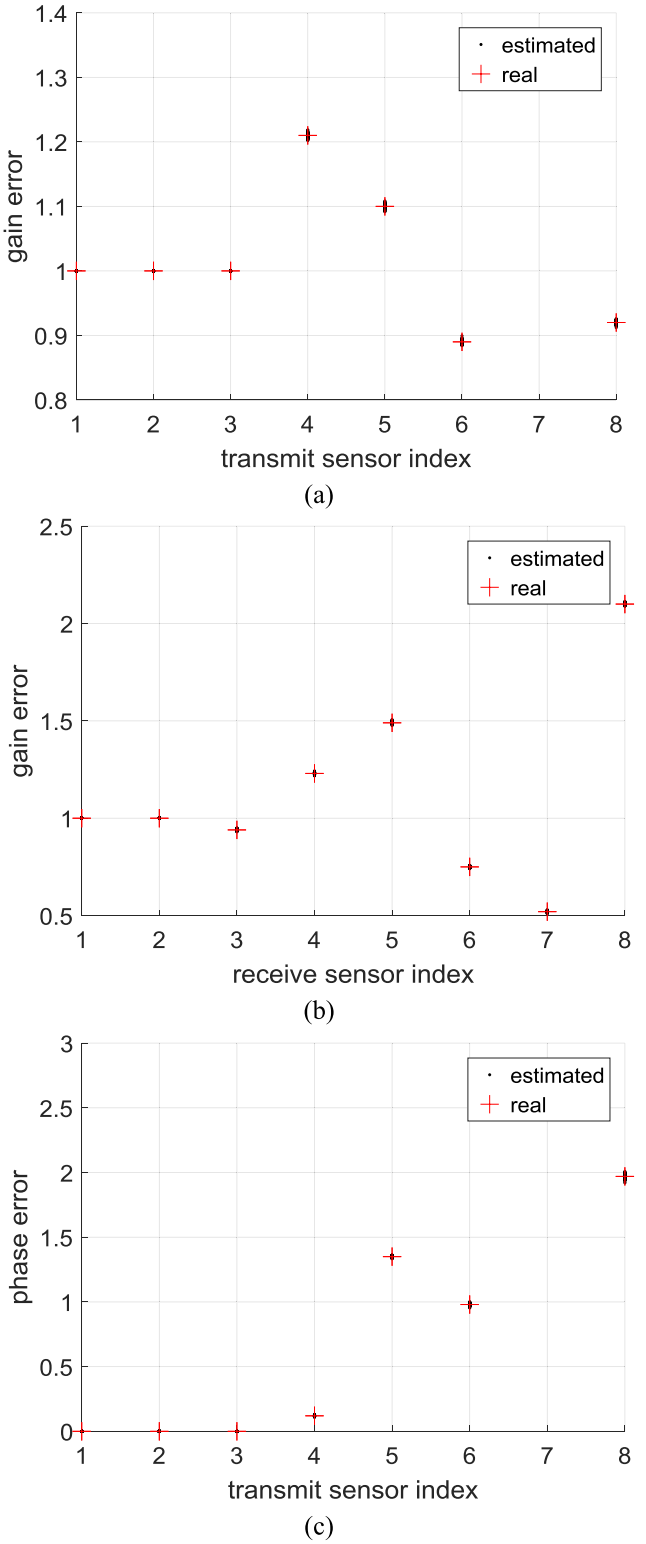

FIGURE 2. Scatter results with SNR = 20 dB(a) transmit gain error. (b) receive gain error.(c) transmit phase error. (d) receive phase error (e) DOD and DOA results.

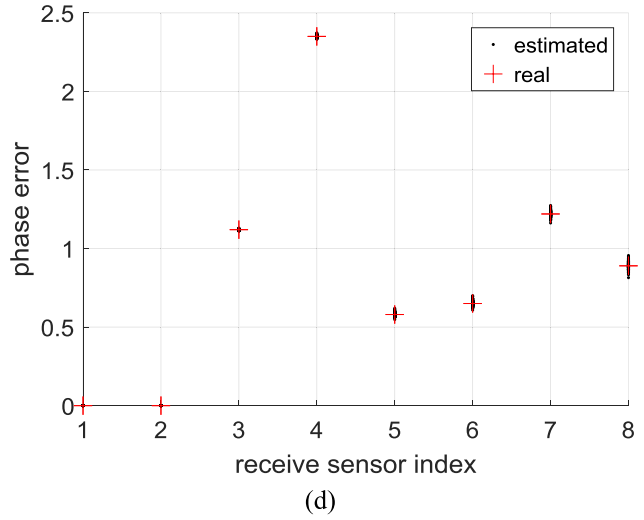

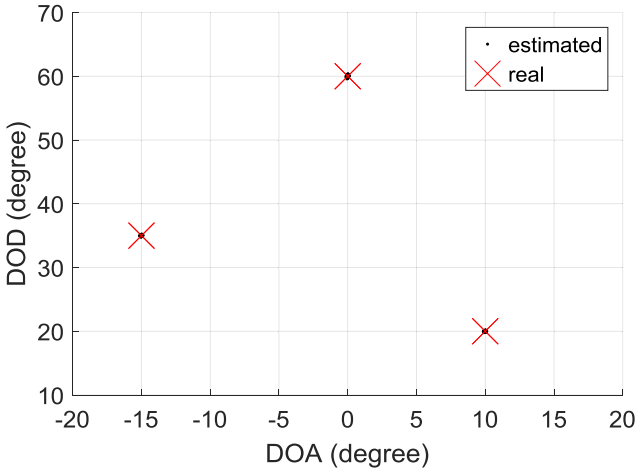

FIGURE 2. *(Continued)* **Scatter results with SNR = 20 dB(a) transmit gain error. (b) receive gain error.(c) transmit phase error. (d) receive phase error (e) DOD and DOA results.**

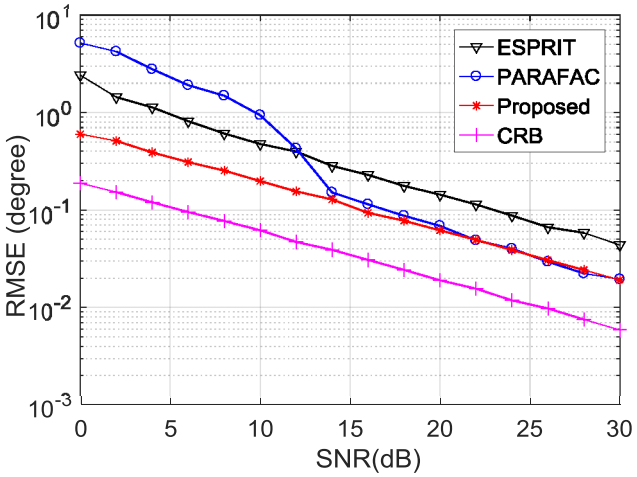

FIGURE 3. **RMSE vs. SNR on direction estimation.**

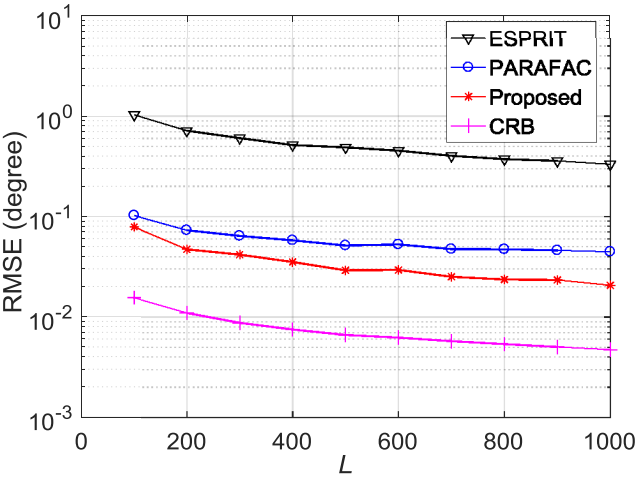

FIGURE 4. **RMSE vs. L on direction estimation.**

The signal-to-noise ratio (SNR) is defined as the signal power to the noise power after matched filtering. The covariance matrix of the spatially noise is $\boldsymbol{Q}$ with the (m, n)-th entity of which is given by $\boldsymbol{Q}(m,n) = e^{-|m-n|\alpha}$, where α is the 'colored' coefficient that control the noise covariance. In each simulation, 200 Monte Carlo rails are carried out. To compare with existing closed-form solution, the performance of the ESPRIT approach in [20] and the PARAFAC approach in [23] are added.

In the first example, we illustrate the scatter results of the proposed PARAFAC estimator with SNR = 20dB, where $\alpha = 0.1$ and $L = 500$ are considered. Fig.2 show the gain-phase errors results and the direction estimation results. It can be seen that the gain-phase errors can be accurately recovered and the angles can be correctly estimated and paired automatically.

In the third example, we test the root mean square error (RMSE) on direction estimation at various SNR (the definition of RMSE is given in [23]), where $\alpha = 0.1$ and $L = 500$. The results are shown in Fig.3. It is seen the PARAFAC method preform worse than ESPRIT at low SNR regions, but it would provide much better performance than the latter when SNR is relative high. Notably, the estimation accuracy of the proposed estimator is much better than ESPRIT and PRAFAC. It shows that the PARAFAC method may provide very close estimation performance to the proposed estimator when SNR is larger than 20dB, as spatially colored noise effect become weak at high SNR regions.

In the fourth example, we compare the RMSE performance at different snapshot number L, where $\alpha = 0.1$ and SNR = 10dB. The result is illustrated in Fig 4. It depicts that the performance of all the algorithms would be improved with increasing L. Besides, tensor methods (PARAFAC and the proposed estimator) offer much better performance than the matrix-based algorithm (ESPRIT), this is caused by the fact that tensor approaches could make full use of the multi-dimensional structure of the array measurement. In addition, the proposed estimator outperform all the compared methods.

In the fifth example, we test how the spatially colored parameter α affect the estimation performance. Fig 5 presents the RMSE comparison results, where L = 500 and SNR = 0dB. It should be noticed that $\boldsymbol{Q} \approx \boldsymbol{I}$ when $\alpha \gg 1$.

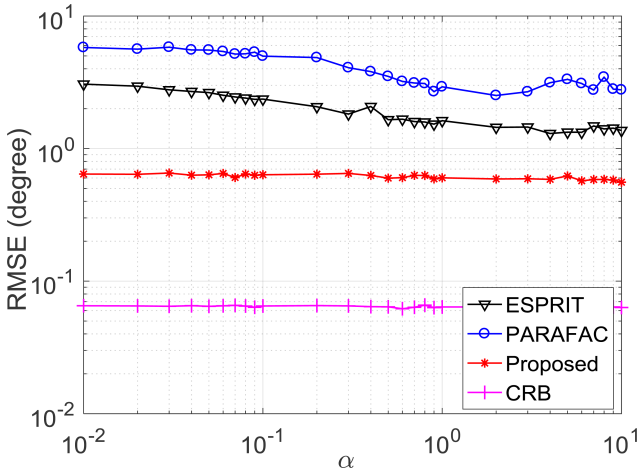

FIGURE 5. RMSE vs. α on direction estimation.

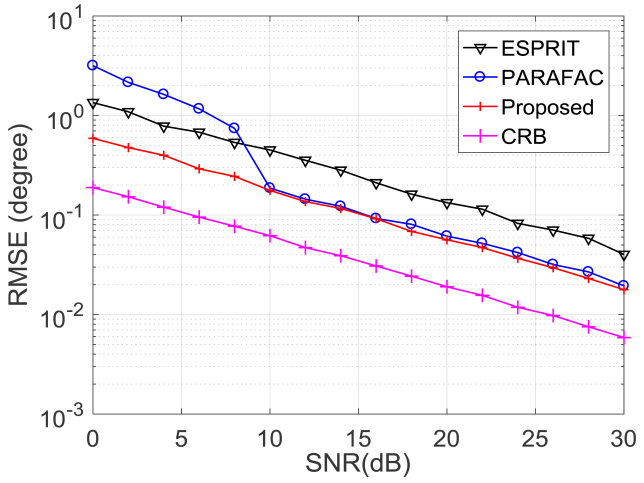

FIGURE 6. RMSE vs. SNR on direction estimation with Gaussian white noise.

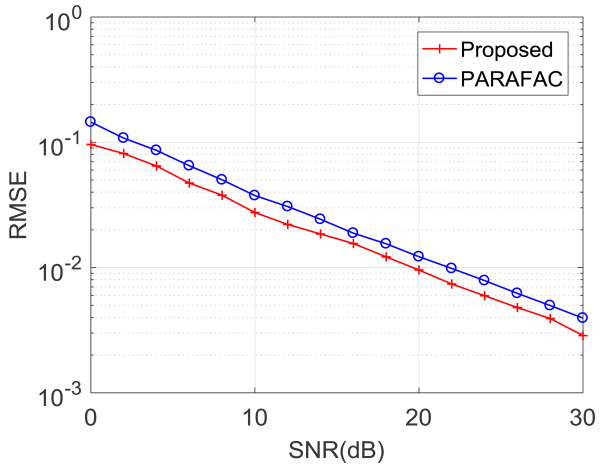

FIGURE 7. RMSE vs. SNR on gain-phase error estimation with Gaussian white noise.

Results show that the proposed algorithm is insensitive to α, as RMSE of the proposed estimator barely changes with α. However, both ESPRIT and PARAFAC are sensitive to the spatially colored noise parameter. As expected, the proposed estimator offers better estimation accuracy than the compared algorithms.

Finally, we compare the RMSE performance of various versus SNR at Gaussian white noise. Simulation conditions are the same to that in the third example. The RMSE performance on direction estimation and RMSE performance on gain-phase error estimation are depicted in Fig. 6 and Fig. 7 (gain-phase error estimation of ESPRIT is not given as it has not been reported in the reference), respectively. A similar observation can be obtained with that with colored noise. The proposed algorithm can achieve better direction estimation performance than all the compared methods.

VI. CONCLUSION

In this paper, we stress the problem of joint DOD and DOA estimation in bistatic MIMO radar with gain-phase errors and spatially colored noise. A fast PARAFAC algorithm is proposed, which is not sensitive to spatially colored noise. Joint DOD and DOA estimation can be easily estimated via Ls technique form the well-calibrated sensors, and the gain-phase errors can be achieved via element-wise operations and Lagrange multipliers. Simulation results show the proposed estimator offers much better estimation performance than the existing close-form solutions. The proposed estimator should have a bright prospect in actual applications.

REFERENCES

[1] H. Wang, L. Wan, M. Dong, K. Ota, and X. Wang, "Assistant vehicle localization based on three collaborative base stations via SBL-based robust DOA estimation," *IEEE Internet Things J.*, vol. 6, no. 3, pp. 5766–5777, Jun. 2019.

[2] F. Wen, J. Wang, J. Shi, and G. Gui, "Auxiliary vehicle positioning based on robust DOA estimation with unknown mutual coupling," *IEEE Internet Things J.*, vol. 7, no. 6, pp. 5521–5532, Jun. 2020, doi: 10.1109/JIOT.2020.2979771.

[3] L. Sun, L. Wan, K. Liu, and X. Wang, "Cooperative-evolution-based WPT resource allocation for large-scale cognitive industrial IoT," *IEEE Trans. Ind. Informat.*, vol. 16, no. 8, pp. 5401–5411, Aug. 2020.

[4] L. Wan, L. Sun, X. Kong, Y. Yuan, K. Sun, and F. Xia, "Task-driven resource assignment in mobile edge computing exploiting evolutionary computation," *IEEE Wireless Commun.*, vol. 26, no. 6, pp. 94–101, Dec. 2019.

[5] B. Liao, "Fast angle estimation for MIMO radar with nonorthogonal waveforms," *IEEE Trans. Aerosp. Electron. Syst.*, vol. 54, no. 4, pp. 2091–2096, Aug. 2018.

[6] T. Liu, F. Wen, J. Shi, Z. Gong, and H. Xu, "A computationally economic location algorithm for bistatic EVMS-MIMO radar," *IEEE Access*, vol. 7, pp. 120533–120540, 2019.

[7] F. Wen and J. Shi, "Fast direction finding for bistatic EMVS-MIMO radar without pairing," *Signal Process.*, vol. 173, Aug. 2020, Art. no. 107512.

[8] T. Liu, F. Wen, L. Zhang, and K. Wang, "Off-grid DOA estimation for colocated MIMO radar via reduced-complexity sparse Bayesian learning," *IEEE Access*, vol. 7, pp. 99907–99916, 2019.

[9] M. Haardt, F. Roemer, and G. Del Galdo, "Higher-order SVD-based subspace estimation to improve the parameter estimation accuracy in multidimensional harmonic retrieval problems," *IEEE Trans. Signal Process.*, vol. 56, no. 7, pp. 3198–3213, Jul. 2008.

[10] Y. Cheng, R. Yu, H. Gu, and W. Su, "Multi-SVD based subspace estimation to improve angle estimation accuracy in bistatic MIMO radar," *Signal Process.*, vol. 93, no. 7, pp. 2003–2009, Jul. 2013.

[11] X. Wang, L. Wan, M. Huang, C. Shen, and K. Zhang, "Polarization channel estimation for circular and non-circular signals in massive MIMO systems," *IEEE J. Sel. Topics Signal Process.*, vol. 13, no. 5, pp. 1001–1016, Sep. 2019.

[12] F. Wen, J. Shi, and Z. Zhang, "Joint 2D-DOD, 2D-DOA, and polarization angles estimation for bistatic EMVS-MIMO radar via PARAFAC analysis," *IEEE Trans. Veh. Technol.*, vol. 69, no. 2, pp. 1626–1638, Feb. 2020.
[13] X. Wang, W. Wang, J. Liu, X. Li, and J. Wang, "A sparse representation scheme for angle estimation in monostatic MIMO radar," *Signal Process.*, vol. 104, pp. 147–152, Apr. 2014.
[14] X. Wang, L. Wang, X. Li, and G. Bi, "Nuclear norm minimization framework for DOA estimation in MIMO radar," *Signal Process.*, vol. 135, pp. 147–152, Jun. 2017.
[15] X. P. Wang, M. Huang, X. Wu, and G. Bi, "Direction of arrival estimation for MIMO radar via unitary nuclear norm minimization," *Sensors*, vol. 17, no. 4, pp. 939–954, Nov. 2017.
[16] F. Wen, X. Xiong, and Z. Zhang, "Angle and mutual coupling estimation in bistatic MIMO radar based on PARAFAC decomposition," *Digit. Signal Process.*, vol. 65, pp. 1–10, Jun. 2017.
[17] C. Zhou, Y. Gu, S. He, and Z. Shi, "A robust and efficient algorithm for coprime array adaptive beamforming," *IEEE Trans. Veh. Technol.*, vol. 67, no. 2, pp. 1099–1112, Feb. 2018.
[18] C. Zhou, Y. Gu, X. Fan, Z. Shi, G. Mao, and Y. D. Zhang, "Direction-of-arrival estimation for coprime array via virtual array interpolation," *IEEE Trans. Signal Process.*, vol. 66, no. 22, pp. 5956–5971, Nov. 2018.
[19] J. Li, X. Zhang, R. Cao, and M. Zhou, "Reduced-dimension MUSIC for angle and array gain-phase error estimation in bistatic MIMO radar," *IEEE Commun. Lett.*, vol. 17, no. 3, pp. 443–446, Mar. 2013.
[20] Y. D. Guo, Y. S. Zhang, and N. N. Tong, "ESPRIT-like angle estimation for bistatic MIMO radar with gain and phase uncertainties," *Electron. Lett.*, vol. 47, no. 17, pp. 996–997, Aug. 2011.
[21] C. Chen and X. Zhang, "Joint angle and array gain-phase errors estimation using PM-like algorithm for bistatic MIMO radar," *Circuits, Syst., Signal Process.*, vol. 32, no. 3, pp. 1293–1311, Jun. 2013.
[22] J. Li, M. Jin, Y. Zheng, G. Liao, and L. Lv, "Transmit and receive array gain-phase error estimation in bistatic MIMO radar," *IEEE Antennas Wireless Propag. Lett.*, vol. 14, pp. 32–35, 2015.
[23] J. Li, X. Zhang, and X. Gao, "A joint scheme for angle and array gain-phase error estimation in bistatic MIMO radar," *IEEE Geosci. Remote Sens. Lett.*, vol. 10, no. 6, pp. 1478–1482, Nov. 2013.
[24] L. Jianfeng and Z. Xiaofei, "A method for joint angle and array gain-phase error estimation in bistatic multiple-input multiple-output non-linear arrays," *IET Signal Process.*, vol. 8, no. 2, pp. 131–137, Apr. 2014.
[25] M. Jin, G. Liao, and J. Li, "Joint DOD and DOA estimation for bistatic MIMO radar," *Signal Process.*, vol. 89, no. 2, pp. 244–251, Feb. 2009.
[26] J. Chen, H. Gu, and W. Su, "A new method for joint DOD and DOA estimation in bistatic MIMO radar," *Signal Process.*, vol. 90, no. 2, pp. 714–718, Feb. 2010.
[27] H. Jiang, J.-K. Zhang, and K. M. Wong, "Joint DOD and DOA estimation for bistatic MIMO radar in unknown correlated noise," *IEEE Trans. Veh. Technol.*, vol. 64, no. 11, pp. 5113–5125, Nov. 2015.
[28] F. Wen, X. Xiong, J. Su, and Z. Zhang, "Angle estimation for bistatic MIMO radar in the presence of spatial colored noise," *Signal Process.*, vol. 134, pp. 261–267, May 2017.
[29] W.-B. Fu, T. Su, Y.-B. Zhao, and X.-H. He, "Joint estimation of angle and Doppler frequency for bistatic MIMO radar in spatial colored noise based on temporal-spatial structure," *J. Electron. Inf. Technol.*, vol. 33, no. 7, pp. 1649–1654, Jul. 2011.
[30] F. Wen, Z. Zhang, and G. Zhang, "Joint DOD and DOA estimation for bistatic MIMO radar: A covariance trilinear decomposition perspective," *IEEE Access*, vol. 7, pp. 53273–53283, 2019.
[31] S. Hong, H. Ke, X. Wan, and F. Cheng, "Covariance differencing-based matrix decomposition for coherent sources localisation in bi-static multiple-input–multiple-output radar," *IET Radar, Sonar Navigat.*, vol. 9, no. 5, pp. 540–549, Jun. 2015.